The Circulation of the Depth-integrated Flow around an Island with Application to the Indonesian Throughflow

ROXANA C. WAJSOWICZ

The Institute of Low Temperature Science, Hokkaido University, Sapporo, Japan

ABSTRACT

Godfrey's *Island Rule* is rederived in terms of the barotropic streamfunction for flow in a stratified ocean with a rigid lid. Modifications to include bottom topography and frictional effects along eastern boundaries are derived. The "Island Rule" has an important application in describing the net transport through the Indonesian seas, that is the Indonesian Throughflow. The original rule, derived from a Sverdrup model, yielded an annual mean throughflow of 16 ± 4 Sv (Sv $\equiv 10^6$ m^3 s^{-1}). Observations of depth-integrated steric height differences indicate that frictional effects within the Indonesian seas will reduce this value by the order of 2 Sv. The reduction estimated from a frictional channel model depends on the parameterization and boundary conditions adopted, and ranges from 5%–20%. Topographic effects could give an increase in transport. For example, if the archipelago is represented as a simple sill, then warmer water on the Pacific slope than on the Indian slope would produce an increase in transport.

A diagnostic island rule for describing interannual variations is proposed. This rule expresses the throughflow as a line integral of the wind stress from the tip of Iria-Jaya along a line of latitude across the Pacific down the South American coast back along a line of latitude across the Pacific to the southern tip of Australia and up Australia's west coast, the original rule, plus a modulation due to the difference between the depth-integrated pressure on the Australian coast at the northern and southern entrances to the Indonesian seas in excess of that required to balance the alongshore wind stress. Frictional and hydraulic effects, which could produce an excess pressure difference, are illustrated with a fine-resolution GCM.

1. Introduction

Godfrey (1989) explicitly derived an *Island Rule* based on a Sverdrup model with simple western boundary-layer dynamics, which gave the transport around a midocean island. A similar formula had been adopted by Veronis (1973) but not explicitly stated. The rule is of topical interest in its application to quantifying the magnitude of the Indonesian throughflow and the forcing, which determines its absolute value and variability. From the island rule, the mean depth-integrated throughflow is driven by the Sverdrup transport integrated across the Pacific and meridionally averaged over the latitudes of Australia–Papua New Guinea (PNG) plus a component due to integrating the alongshore wind stress around Australia–PNG. Numerical general circulation models of the mean global ocean circulation, which incorporate the passages of the Indonesian archipelago as a wide and deep channel, yield depth-integrated transports of about 15 Sv (e.g. Cox 1975; Semtner and Chervin 1988; and Hirst and Godfrey 1993). This is in close agreement with Godfrey's island rule estimate of 16 ± 4 Sv (Sv $\equiv 10^6$ m^3 s^{-1}). No direct observational confirmation of this value has been published. However, Gordon (1986) found that about 10 Sv would be consistent with balancing the global heat and salinity budgets, assuming the Indonesian seas were the only route for the warm surface waters to transport their heat from the Pacific to the Indian Ocean. Also, Godfrey (1989) calculated a depth-integrated steric height difference between the west coast of Australia and Sumatra of 30 m^2, using Levitus' (1982) climatological hydrography. For latitudes 9°–12°S, this implies a geostrophic throughflow of 10–13 Sv.

More recent efforts have concentrated on describing the variability of the throughflow on seasonal and interannual time scales, for example, Kindle et al. (1989), Murray and Arief (1988), and Inoue and Welsh (1993). Wyrtki (1987) hypothesized that the throughflow is driven by a pressure head between the Pacific and Indian oceans, and looked for correlation between its magnitude and the sea-level difference between Davao, Philippines, and Darwin, Australia. Davao was found to be a poor indicator of sea-level variability in the western Pacific, as the signal is contaminated by the high-frequency fluctuations of the unstable Mindanao Current and other off-equatorial signals, as noted by Clarke (1991). These studies have not answered the

Corresponding author address: Dr. Roxana C. Wajsowicz, Mail Code 971, Oceans and Ice Branch, NASA/Goddard Space Flight Center, Greenbelt, MD 20771.

fundamental question of what sets the pressure head between the Pacific and Indian oceans.

A mathematical framework based on the equations of motion and boundary conditions set out in section 2 is used to reconcile the various hypotheses and descriptions in sections 3 and 4. Godfrey's island rule, which assumes any western boundary to the ocean is remote, is rederived in section 3 with several alternative expressions allowing for multiple islands and topography. If an island lies within a western boundary layer, then frictional effects will be important along the island's west as well as east coast. This is discussed in section 4, and estimates are made for Stommel and Munk parameterizations of friction. A diagnostic rule for describing interannual variations in the throughflow is proposed. The rule is formulated to show how the dynamics of the Indonesian seas will modulate the "ideal" value given by the Pacific/Australian wind stress. The modulation is due to the unknown factor of the change in depth-integrated pressure along Australia's west coast, which is in excess of that required to balance the alongshore wind stress. The excess could be due to frictional or hydraulic effects for example. Although it may not be feasible to investigate depth-integrated pressure variations between the tip of Iria-Jaya and, say, Darwin based on past records, it could be a future project. Also, such a relationship could be investigated in the many numerical modeling studies underway. Finally, in section 5, several aspects of the dynamics of the Indonesian seas are briefly illustrated through results from a fine-resolution GCM, which had been run for ENSO studies.

2. Basic equations of motion and boundary conditions

The existence of a streamfunction, ψ for the depth-averaged flow, given by

$$\psi_x = \int_{-H}^0 v\,dz, \quad \psi_y = -\int_{-H}^0 u\,dz, \quad (2.1)$$

where $z = -H(x, y)$ is the ocean floor, may be deduced by vertically integrating the continuity equation and making the rigid-lid approximation ($w = 0$ at the surface). The depth-averaged, linear, horizontal momentum equations for a stratified ocean, subject to a wind stress $\mathbf{\tau}$, are

$$-\frac{1}{H}\nabla_h \times (\psi_t\mathbf{k}) - \frac{f}{H}\nabla_h\psi$$

$$= -\nabla_h P + \mathcal{P}\nabla_h H + \frac{\mathbf{\tau}}{\rho_o H} + \frac{\mathbf{F}}{H}, \quad (2.2)$$

where

$$P = \frac{1}{\rho_o H}\int_{-H}^0 p\,dz = \frac{p_s}{\rho_o} + \frac{g}{\rho_o H}\int_{-H}^0 \int_z^0 \rho\,dz'dz, \quad (2.3a)$$

$$\mathcal{P} = \frac{1}{H}\left(\frac{p_b}{\rho_o} - P\right) = \frac{g}{\rho_o H^2}\int_{-H}^0\left\{H\rho - \int_z^0 \rho\,dz'\right\}dz, \quad (2.3b)$$

and where ∇_h is the horizontal gradient operator, and p_s, p_b are the surface and bottom pressures, respectively. The depth-integrated frictional stress is represented by the term $\mathbf{F}$; it is not necessary to specify its exact form for the following calculations. Performing the operation curl $\equiv \mathbf{k} \cdot \nabla_h \times$ on (2.2) yields the barotropic vorticity equation

$$\nabla_h \cdot \left(\frac{1}{H}\nabla_h\psi_t\right) - J\left[\frac{f}{H}, \psi\right]$$

$$= J[\mathcal{P}, H] + \text{curl}\,\frac{\mathbf{\tau}}{\rho_o H} + \text{curl}\,\frac{\mathbf{F}}{H}, \quad (2.4)$$

where

$$J[a, b] = a_x b_y - a_y b_x. \quad (2.5)$$

For a closed, simply connected basin, the form of $\mathbf{F}$ is chosen so that (2.4) is a prognostic equation for ψ, given the boundary condition that ψ is a constant, usually taken as zero, along the basin's boundary. The requirement on the form of $\mathbf{F}$ for the solution to be uniquely determined is given in the Appendix. If $\mathbf{F}$ involves derivatives of ψ higher than the first, then further boundary conditions on ψ will need to be specified. For example, if $\mathbf{F} = -A_M\nabla^2[\nabla \times (\psi\mathbf{k})]$, then the no-slip condition that the normal component of $\nabla_h\psi$ is zero on the boundary is usually chosen. The uniqueness of the solution for variable bottom topography and stratification will depend of course on the uniqueness of solution to the prognostic equation for ρ and boundary conditions.

If the domain includes an island, then (2.4) is solved with the extra boundary condition that there is no normal flow, and so $\psi = \psi_0(t)$ on the island's boundary. A prognostic equation to determine $\psi_0(t)$ uniquely is obtained by integrating (2.2) around its coastline ∂I and assuming P is single-valued around the island, which gives

$$-\oint_{\partial I} \frac{1}{H}\nabla_h \times (\psi_t\mathbf{k}) \cdot d\mathbf{l}$$

$$= \oint_{\partial I} \mathcal{P}\nabla_h H \cdot d\mathbf{l} + \oint_{\partial I} \frac{1}{H}\left(\frac{\mathbf{\tau}}{\rho_o} + \mathbf{F}\right) \cdot d\mathbf{l}, \quad (2.6)$$

where $d\mathbf{l}$ is the infinitesimal displacement vector tangent to ∂I. The Coriolis contribution has been eliminated as the no normal flow boundary condition implies $\nabla_h\psi \cdot d\mathbf{l} \equiv 0$.

The depth-averaged pressure $\rho_o P$ is determined by solving the elliptic equation given by $\nabla_h \cdot [H \times (2.2)]$, namely,

$$\nabla_h \cdot (H\nabla_h P) = f\nabla_h^2 \psi + \beta\psi_y + \nabla_h \cdot (\mathcal{P}H\nabla_h H)$$
$$+ \nabla_h \cdot \left(\frac{\mathbf{r}}{\rho_o} + \mathbf{F}\right). \quad (2.7)$$

The time-dependency of P is contained in its boundary conditions, which express Kelvin waves propagating information about changes in P along the coasts. Applying the operator $(\mathbf{n} \cdot \partial_t + \mathbf{l} \cdot f)$ to (2.2), and noting $\psi_l \equiv 0$ on a boundary, gives

$$\nabla_h P_t \cdot \mathbf{n} + f\nabla_h P \cdot \mathbf{l} = (\mathbf{n} \cdot \partial_t + \mathbf{l} \cdot f)$$
$$\times \left\{\mathcal{P}\nabla_h H + \frac{\mathbf{r}}{\rho_o H} + \frac{\mathbf{F}}{H}\right\} \quad \text{on} \quad \partial B, \quad (2.8)$$

where $\mathbf{n}$, $\mathbf{l}$ are the normal and tangent vectors to the coast ∂B, defined so that $\mathbf{l} = \mathbf{k} \times \mathbf{n}$. The time scale of variations in P will depend on the baroclinic phase speeds of the vertical modes of the system, and so P will vary on a quite different time scale from ψ.

The quantities P, $\mathcal{P}$ given in (2.3) are best illustrated by considering a two-layer system with a rigid lid. Suppose fluid of density ρ_1 and mean depth H_1 overlies fluid of density ρ_2 and mean depth $H_2(\equiv H - H_1)$, and let η denote a positive perturbation to the interfacial height. Assuming the system is hydrostatic, then

$$\frac{p_b}{\rho_2} = \frac{p_s}{\rho_2} + gH - g'(H_1 - \eta), \quad (2.9a)$$

and

$$P = \frac{p_s}{\rho_2} + \frac{gH}{2} - \frac{g'}{2H}(H_1^2 + 2H_1H_2 - \eta^2), \quad (2.9b)$$

where $g' \equiv g(\rho_2 - \rho_1)/\rho_2$ is the reduced gravity. Therefore, from (2.3b),

$$\mathcal{P} = \frac{g}{2} - \frac{g'}{2H^2}(H_1^2 - 2H\eta + \eta^2). \quad (2.9c)$$

The time variation of p_b and P will be functions of p_s, η and thus functions of the external and internal mode wave speeds. The time variation of $\mathcal{P}$ is just a function of the internal mode speed.

Analytic solutions for the circulation around an island ψ_0 can be found if the explicit time derivatives in (2.4) and (2.6) are neglected. For a flat-bottomed ocean, ψ will adjust to a time-varying wind-stress curl or bottom-pressure torque via barotropic Rossby waves of frequency $\omega = -(\beta p)/(p^2 + q^2)$ for wavenumber (p, q). Therefore, the adjustment time scale outside the western boundary layer to a wind stress of scale L in a basin of scale B is $B/(\beta L^2)$. For $B \sim 4 \times 10^4$ km, $L \sim 2 \times 10^3$ km, $\beta \sim 2 \times 10^{-11}$ m^{-1} s^{-1}, the time scale is 8 days. The other time scale of importance is that to dissipate vorticity in a western boundary layer. In a Munk model with viscosity coefficient A_M, the equilibration time scale for a western boundary layer is $(\beta^2 A_M)^{-1/3}$, which for $A_M \sim 10^4$ m^2 s^{-1} is 7 days.

Therefore, if the oceans were flat and simply connected, the streamfunction response to large-scale seasonal wind-stress variations could be calculated from (2.4) ignoring the time-derivative term. The time-derivative term in (2.6) is negligible on time scales greater than $R/(\beta^2 A_M)^{1/3}$, where R is the ratio of the length of the island's boundary to its meridional extent. Explicit expressions for ψ_0 are derived in section 3 and are independent of the exact specification of $\mathbf{F}$, provided it is assumed that vorticity is dissipated at the latitude of creation in the western boundary layer. If the ocean basin has variable topography, then the adjustment time scale for ψ will be much longer if the barotropic-topographic Rossby wave speed is reduced significantly. This will occur if there are regions where meridional variations in H significantly reduce the effective β, that is, $|1 - (fH_y)/(\beta H)| \ll 1$, or if there are regions where $0 < |fH_x|/(\beta H) \ll 1$. An expression for ψ_0 is derived in section 3 for explicitly varying topography. The topographic rule describes the response to wind stress and bottom pressure variations on time scales longer than the barotropic–topographic Rossby adjustment time scale and western boundary layer equilibration scale. The $\mathcal{P}\nabla_h H$ variations could be due to explicit buoyancy forcing or to the baroclinic adjustment associated with the response to varying wind stress. In the latter case, the topographic rule could be used in a diagnostic mode only. On time scales longer than it takes baroclinic Rossby waves to cancel the wind-driven flow at depth, ψ_0 is given in terms of the explicit wind and thermohaline forcing.

3. Island circulation for a remote western boundary

An example of the geometry considered is shown in Fig. 1. Any western boundary to the ocean is sufficiently
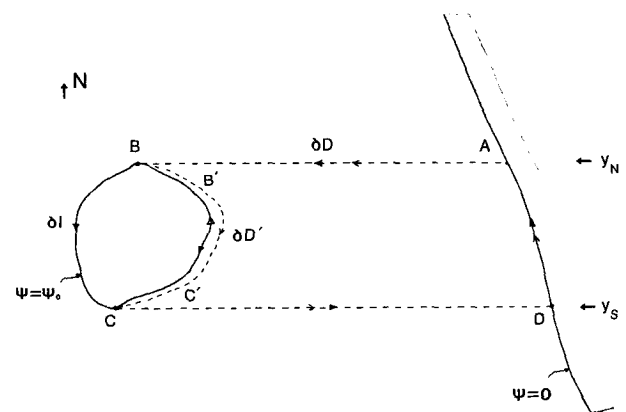

FIG. 1. The geometry and paths used to derive the island rule (3.3). The path ∂D ($\rightarrow$) is from point A westward to B, then southward along the east coast of the island to C, then eastward to D, and northward along the basin's east coast to A. The path $\partial D'$ ($\rightarrow$) is the same as ∂D with the leg BC replaced by $B'C'$ lying on the interior edge of the western boundary layer. The path ∂I ($\rightarrow$) is anticlockwise around the island boundary.

remote from the island under consideration that frictional effects on the island's boundary are assumed negligible except along its east coast. In both this section and the next, H is assumed to take a constant value H_0, unless stated otherwise. The depth H_0 can represent the actual depth of a flat-bottomed ocean, in which case the value of ψ on the island ψ_0 describes the response to a wind stress varying on time scales longer than the barotropic Rossby adjustment scale. Alternatively, if there is a level of no motion below which the pressure gradients are zero, then H_0 can be interpreted as its depth, but then ψ_0 is the response to a wind stress varying on time scales longer than the baroclinic Rossby adjustment scale. For the sake of argument, the ensuing discussion will be for a flat-bottomed ocean. The modification due to explicitly varying topography is given in (3e).

a. Original island rule

Integrating (2.4) over the domain D (denoted by ABCD in Fig. 1) with boundary ∂D, neglecting the time-derivative term and applying Stokes' theorem, yields

$$-(f_N - f_S)\psi_0 = \oint_{\partial D} \frac{\boldsymbol{\tau} \cdot \mathbf{d}l}{\rho_0} + \oint_{\partial D} \mathbf{F} \cdot \mathbf{d}l, \quad (3.1)$$

where f_N, f_S are the values of the Coriolis parameter at y_N, y_S, the northernmost and southernmost latitudes of the island, respectively, and $\mathbf{d}l$ is an infinitesimal line element tangential to ∂D. From (2.6), neglecting the time-derivative term,

$$\oint_{\partial I} \frac{\boldsymbol{\tau} \cdot \mathbf{d}l}{\rho_0} = -\oint_{\partial I} \mathbf{F} \cdot \mathbf{d}l. \quad (3.2)$$

Therefore, if it is assumed that frictional effects are only significant over the western boundary layer, specifically the section BC of both ∂D and ∂I in Fig. 1, then the friction terms may be eliminated between (3.1) and (3.2) giving an explicit expression for ψ_0; namely,

$$\psi_0(t) = \frac{-1}{(f_N - f_S)} \oint_{\partial D + \partial I} \frac{\boldsymbol{\tau}(x, y, t) \cdot \mathbf{d}l}{\rho_0}. \quad (3.3)$$

The expression (3.3) is just the "Island Rule" derived by Godfrey (1989) for the climatological mean circulation assuming there existed a level of no motion above all of the topography. A more physically intuitive form of the island rule (cf. an aerofoil) is obtained by noting that integrating (2.4) over the domain with boundary $\partial D'$ (AB'C'DA in Fig. 1, where B' $\rightarrow$ C' lies just outside the western boundary layer) gives

$$(f_N - f_S)\overline{\psi_D} = -\oint_{\partial D'} \frac{\boldsymbol{\tau} \cdot \mathbf{d}l}{\rho_0}, \quad (3.4)$$

where $\overline{\psi_D}$ is the meridional average over the latitudes of the island of the net northward Sverdrup transport between the island and the boundary to the east.

Therefore, assuming that the western boundary layer is sufficiently thin that the integral of the wind stress around $\partial D'$ may be performed around ∂D, then (3.3) may be rewritten as

$$\psi_0(t) = \overline{\psi_D(t)} - \frac{1}{(f_N - f_S)} \oint_{\partial I} \frac{\boldsymbol{\tau}(x, y, t) \cdot \mathbf{d}l}{\rho_0}. \quad (3.5)$$

It is important to note the implicit assumptions contained in assuming that the frictional term in the line integrals along ∂D and ∂I is only important along section BC. For ∂I, this implies that the island is sufficiently remote from any western boundary to the ocean that no part of the island lies within its boundary layer. For ∂D, it implies that vorticity is dissipated at the latitude of creation in the western boundary layer, so that the boundary-layer thickness tends to zero at the island tips.

b. Multiple island rule

The dependence of ψ_0 on the local wind stress and that to the east enables a ready calculation of ψ on a chain of islands (see Fig. 2). Using a similar method to that previously described, the value of ψ on an island to the west of first is

$$\psi_1(t) = \frac{Y_O}{Y'} \psi_0(t) + \frac{Y_E}{Y'} \overline{\psi_E(t)}$$

$$- \frac{1}{(f_{N'} - f_{S'})} \oint_{\partial G + \partial I'} \frac{\boldsymbol{\tau}(x, y, t) \cdot \mathbf{d}l}{\rho_0}, \quad (3.6)$$

where Y' is the meridional extent of the westward island, and Y_O is that of the overlap of the two islands. The meridionally averaged Sverdrup transport over the latitudes at which the westward island is exposed to the east coast of the basin is $\overline{\psi_E}$, and the meridional extent of this exposure is $Y_E (= Y' - Y_O)$. The paths $\partial I'$, ∂G are the boundary of the westward island and around the gap between the two islands (see Fig. 2).
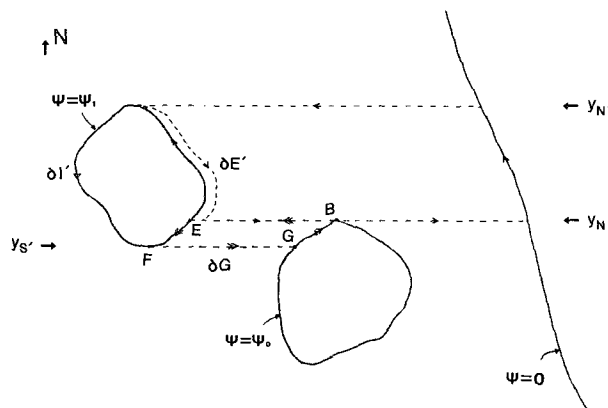

FIG. 2. The geometry and paths used to derive the multiple, overlapping island rule (3.6), where $Y_E = y_{N'} - y_N$, $Y_O = y_N - y_{S'}$.

The difference in f between the northernmost and southernmost tips of the westward island is $f_{N'} - f_{S'}$.

c. Application to the Indonesian throughflow

If the Indonesian sills were sufficiently deep, so that the JEBAR (Joint Effect of Baroclinicity and Relief; e.g., see Huthnance 1984) term $J[\mathcal{P}, H]$ in (2.4), and the bottom pressure term $\oint_{\partial I} \mathcal{P} \nabla_h H \cdot d\mathbf{l}$ in (2.6), could be neglected, and if the straits were sufficiently wide, so that frictional effects along the west coasts of Australia–PNG, Sulawesi, etc. could be neglected, then a combination of (3.3) and (3.6) could be used to give an estimate of the magnitude and variability of the depth-integrated Indonesian throughflow. Ignoring New Zealand, the magnitude and variability of the net throughflow would depend only on the zonal wind stress across the Pacific at the northernmost and southernmost latitudes of Australia–PNG and the alongshore wind stress along the west coasts of Australia and South America. This simple result would be invalidated only if the East Australia Current and equatorial currents were highly nonlinear, so modifying (2.4) and (2.6), or if frictional effects were important other than in the western boundary layer. A simple, flat-bottomed numerical GCM of the Indo–Pacific region forced by Hellerman and Rosenstein's (1983) climatological monthly mean wind stress just over the Pacific described in Wajsowicz (1993a) gave good agreement with (3.5) for Australia–PNG, but less so with (3.6) for Halmahera, a small island spanning the equator west of PNG. Its meridional extent is not sufficient for dissipation in its western boundary layer to dominate that in the vicinity.

The preceding suggests that useful insight into the throughflow variability could be obtained from calculating the wind-stress integral in (3.3), or (3.6) if New Zealand is taken into account, from available wind-stress data. The region that sets the mean value and that which gives the variability on relevant time scales could be identified. Evaluation of the integral using Hellerman and Rosenstein's (1983) monthly mean wind stresses on a $1° \times 1°$ grid gives a mean throughflow of 18 Sv. The value would be about 2 Sv lower if New Zealand were ignored. The contribution from along $45°$–$55°$S dominates the integral, accounting for about 11 Sv. The contribution from the equatorial zonal wind stress is about 6 Sv. For modeling studies, this implies that to get the full magnitude of the annual mean throughflow, the domain of a numerical model would have to extend from the equator to south of Australia, or to have open boundary conditions. The annual cycle dominates the variability with a peak-to-peak amplitude of about 6 Sv. The integral is a minimum in February and a maximum in July. The variation is chiefly attributable to the monsoonal winds over NW Australia and PNG.

Investigation of the wind-stress integral on inter-

annual time scales is difficult. The study of the ENSO phenomenon has led to quality datasets of the tropical regions, but those for $45°$–$55°$S are sparse. Data from numerical weather prediction models are a possibility, but most are currently undergoing reanalysis. Results using the European Centre for Medium-Range Weather Forecasting's winds at 1000 mb for the period 1980–86 and those of the Japan Meteorological Agency for 1987–89, and COADS (Comprehensive Ocean–Atmosphere Data Set) pseudo-wind stresses for 1970–79 are described in Wajsowicz (1983c). Briefly, there is a strong interannual signal with a peak-to-peak amplitude of $\sim$5 Sv. Typically, there is a sharp drop, coinciding with the onset of an ENSO event, followed by a gradual increase. The variability results as much from the variation in zonal wind stress in the south Pacific as from that along the equator.

d. Depth-integrated pressure differences

In discussing the Indonesian throughflow and its variability, the pressure head between the Pacific and Indian oceans is often hypothesized as driving the time-mean throughflow and variations of sufficiently low frequency for geostrophic balance to be assumed (e.g. Wyrtki 1987). Wyrtki (1987) did not derive an explicit equation relating the variation in sea level difference between Davao and Darwin to variations in the throughflow, but it is likely that his calculations were motivated by considering the cross-stream component of (2.2). Integrating across the stream between the Asian and Australian continents (see Fig. 3), assuming geostrophic balance, and neglecting the frictional and wind-stress terms, yields

$$H_0 \Delta P_{EG} = -\frac{1}{2} (f_N + f_{S'})\psi_0. \qquad (3.7)$$

Also, it is assumed that the channel is sufficiently narrow that either f or $\nabla_h \psi \cdot \mathbf{n}$ is constant. Of course in-
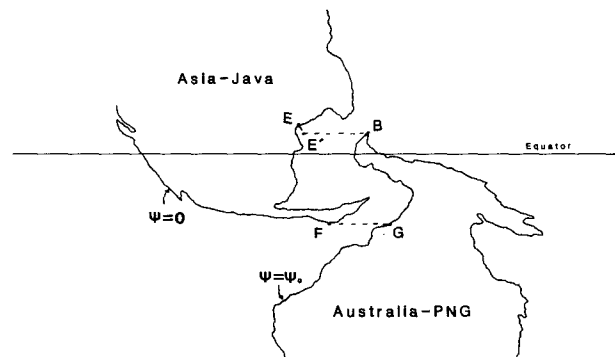

Fig. 3. A schematic of the Indo–Pacific with the connection between the Pacific and Indian oceans represented as a wide channel. The depth-averaged pressure difference, ΔP_{EAST} is the difference between points B and G, and ΔP_{WEST} is the difference between points E and F.

tegrating the time-independent form of (2.2) around similar integrals to those used to derive (3.3) gives a pressure difference ΔP_{EG}, which when equated to (3.7) gives Godfrey's island rule with the extra assumptions already stated.

The depth-integrated pressure difference along a boundary may be calculated from (2.8), if the explicit time-derivative in P can be neglected. This occurs on time scales longer than it takes Kelvin waves to smooth out gradients along the coast. For a continuously stratified ocean, the time scale is infinite, so only the equilibrium pressure head to a steady wind stress can be determined. If the first baroclinic mode dominates, then shorter time scale variations may be described. If the boundary intersects the equatorial waveguide, then the equilibration via equatorial waves must also be taken into account. The *equilibrium* pressure heads along the west Australian and east Asian coasts, due to a *steady* forcing, are given by

$$H_0\Delta P_{\text{EAST}} = \int_G^B \frac{\mathbf{\tau}(x, y)}{\rho_o} \cdot d l, \qquad (3.8a)$$

$$H_0\Delta P_{\text{WEST}} = \int_F^E \left\{ \frac{\mathbf{\tau}(x, y)}{\rho_o} + \mathbf{F} \right\} \cdot d l, \qquad (3.8b)$$

respectively, assuming the ocean is flat and Australia–PNG lies outside the Asian western boundary layer, see Fig. 3. Also, the cross-stream component of $\mathbf{F}$ is assumed negligible in the western boundary layer. The friction integral may be determined in the same way as (3.1), with ∂D replaced by BEGFB in Fig. 3, which on substituting into (3.8b) gives

$$H_0\Delta P_{\text{WEST}} = -(f_N - f_{S'})\psi_0 + \int_{\text{FGBE}} \frac{\mathbf{\tau}(x, y)}{\rho_o} \cdot d l.$$
$$(3.8b')$$

If the time-mean wind stress over the Indonesian seas is negligible compared with that over a similar path length in the Pacific, then the equilibrium depth-integrated pressure difference is directly proportional to the magnitude of the equilibrium depth-integrated throughflow. However, in a *flat-bottomed* ocean, the depth-integrated throughflow magnitude is not set by the pressure difference between the Pacific and Indian oceans as measured along one of the boundaries, but by the Sverdrup transport in the Pacific and the wind stress around Australia–PNG. The P field is determined from the ψ field and may vary on a quite different time scale, as demonstrated by (2.7)–(2.8).

An estimate of ΔP_{WEST} is available from Godfrey's (1989) depth-integrated steric height calculation, relative to 1500 mb, based on Levitus (1982) climatological hydrography. From his Fig. 6a, $HP_{\text{WEST}}/g \approx 100$ m^2 at the Pacific entrance to the Indonesian archipelago and ≈ 50 m^2 at the Indian exit. Hence, ignoring the wind-stress contribution and taking $f_N \approx 0, f_{S'} \approx f(12°S) = 3 \times 10^{-5}$ s^{-1}, then (3.8b') gives

$\psi_0 \lesssim -16$ Sv. The constant of proportionality $(f_N - f_{S'})$ in (3.8b') is very small, and the result is very sensitive to the choices of f, which varies rapidly over equatorial latitudes. A similar consideration holds for (3.7). The small proportionality constants could help explain the poor correlation between throughflow and sea-level difference between Davao and Darwin found by so many authors.

e. Topographic effects

Assuming that the wind stress and bottom-torque variations are on time scales much greater than the barotropic–topographic Rossby adjustment time scale, then an island rule may be derived explicitly for the case of bottom topography that varies arbitrarily, but not zonally along the latitudes of the northernmost and southernmost tips of the island eastward of the island. If H_N, H_S are the depths of the ocean at these latitudes, then following a method similar to deriving (3.3), but retaining the bottom pressure terms in (2.4) and (2.6), yields the *topographic island rule*

$$\left(\frac{f_N}{H_N} - \frac{f_S}{H_S} \right)\psi_0(t) = -\oint_{\partial D + \partial I} \left\{ \mathcal{P}(x, y, t)\nabla_h H \right.$$
$$\left. + \frac{\mathbf{\tau}(x, y, t)}{\rho_o H} \right\} \cdot d l. \qquad (3.9)$$

As well as the actual bottom topography, H may be interpreted as a combination of bottom topography and a level of no motion, below which the pressure gradients are zero, for the equilibrium response to a steady forcing. The level of no motion may intersect the bottom topography because a sill penetrates into the mixed layer, or a level of no motion may not exist in a region because of a deep thermohaline circulation. For the Indonesian throughflow, $f_S < 0, f_N \approx 0$, and the wind-stress integral is positive, so giving $\psi_0 < 0$ in the absence of topographic effects. Since pressure typically increases with depth, the depth-averaged pressure will be less than the bottom pressure, and so $\mathcal{P}$ given by (2.3b) is positive. If $\mathcal{P}$ is uniform over the slopes of a sill between basins of equal depth, then there is no effect on the throughflow magnitude. However, if the west Pacific/eastern Indonesian archipelago is warmer, then $\mathcal{P}$ will typically be less positive over the upslope, that is, where $\nabla_h H \cdot d l < 0$, than over the downslope of the sill. This can be easily seen for a two-layer system by considering (2.9c). If $\rho_1(\text{Pac}) < \rho_1(\text{Ind})$, other quantities being equal, then $\mathcal{P}(\text{Pac}) < \mathcal{P}(\text{Ind})$. Therefore, the integral of $\mathcal{P}\nabla_h H \cdot d l$ over the sill is positive, and so ψ_0 is more negative, and there is an increase in the throughflow magnitude (see Fig. 4). A perturbation that lowers the thermocline in the west Pacific will have the same effect [see (2.9c)]. The result is sensitive to details of topography and the density field, but it does suggest that the throughflow has a modulating effect on the west Pacific warm water
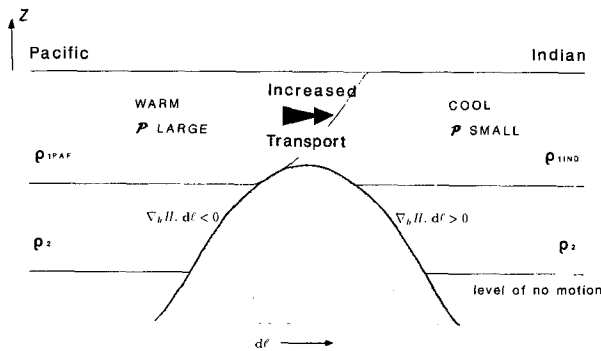
FIG. 4. A schematic of the $\mathcal{P}\nabla_h H$ effect on the Indonesian archipelago.

pool. The throughflow irreversibly transports heat from the Pacific to the Indian Ocean. An increase in heat input into the pool will be compensated to some extent by an increase in heat leaving the pool through the archipelago.

Hirst and Godfrey (1993) report a sensitivity in the depth-integrated throughflow to sill depth in their GCM integrations. For a single channel and sill, the net throughflow was 21–24 Sv for a sill depth in the range 1250–2800 m, and 16 Sv for a depth of 3700 m. Their results suggest that there is a source for a buoyancy-driven flow between the Pacific and Indian Oceans at mid-depth. The floor of the Pacific Ocean is not flat, but slopes upward from the west to east Pacific. Based on numerical GCM studies, Ishizaki (1993) has proposed that this zonal gradient leads to a mid-depth branch of the Pacific thermohaline circulation; such a branch does not exist for the Atlantic Ocean. Rhines and McCready (1989) have noted a similar *hypsometric* effect, confirmed by laboratory experiments. Enhancement of transport due to a $\mathcal{P}\nabla_h H$ effect has also been noted in the context of the Antarctic Circumpolar Current and Drake Passage (e.g., Gill and Bryan 1971).

Equation (3.9) shows the complex correlation that may exist between the time variations in throughflow magnitude and depth-integrated pressure. The weak correlation with pressure variations due to wind-stress forcing, as described by (3.7) and (3.8b'), will be further contaminated by the signal from density variations over the sloping Indonesian topography. The equivalent to (3.7) is somewhat unhelpful, unless it is possible to measure the pressure difference across the stream between the Asian and Australian continents at a point where H does not vary, so giving (3.7).

4. Island circulation for a near–western boundary

a. Island rule with friction

A further theoretical consideration, with important application to the Indonesian throughflow problem, is

the modification to (3.3) if part of the island lies within the basin's western boundary layer (see Fig. 5). In the derivation of (3.3), the frictional terms in (3.1) and (3.2) no longer cancel; there is a contribution from the west coast of the island to the integral along ∂I and part of the integral around ∂D remains if part of the island's east coast lies in the boundary layer. Hence,

$$\psi_0(t) = \frac{-1}{(f_N - f_S)} \oint_{\partial D + \partial I} \frac{\mathbf{r}(x, y, t) \cdot \mathbf{d}l}{\rho_o}$$

$$+ \frac{1}{(f_N - f_S)} \int_{RQP} \mathbf{F} \cdot \mathbf{d}l. \quad (4.1)$$

Considering Fig. 5b, the contribution to the friction integral from the BP leg will be negligible compared to that from the RQB leg if the meridional extent of RQB is much larger than the length BP.
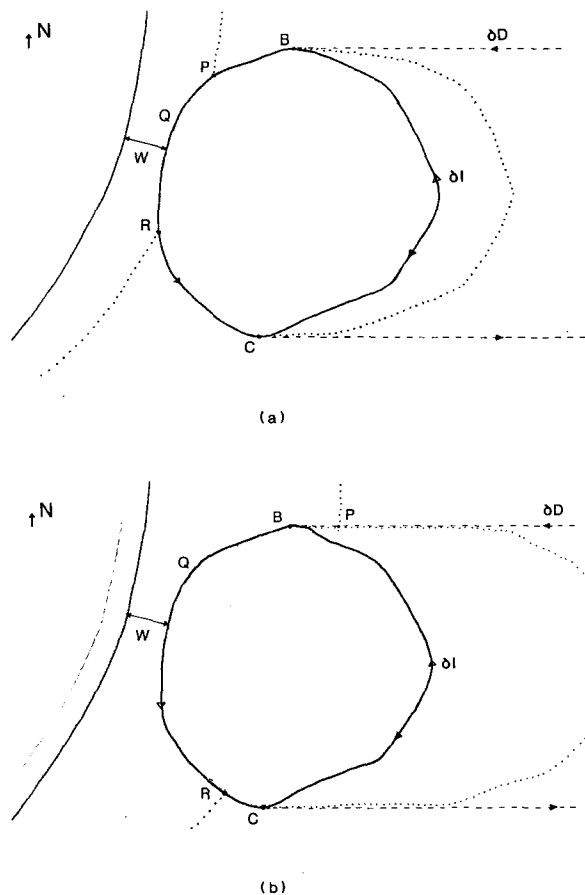

(a)

(b)

FIG. 5. The geometry showing an island lying partially within the basin's western boundary layer. Only part of the island's west coast lies in the layer in (a), but all of its west coast plus part of its east coast in (b). The latitude y_N is P in (a) and B in (b), and the latitude y_S is R in both (a) and (b). The extent of the western boundary layers are denoted by a dotted line. The horizontal scales of the boundary layers have been exaggerated.

b. Estimates for Stommel and Munk friction

From (4.1), the value of ψ_0 will depend on the form of F. An estimate of the decrease in ψ_0 from ψ_{max}, the value given by (3.3), can be made for Stommel and Munk forms of friction as follows. Suppose the area between the island and boundary to the west is modeled by a single channel of width W and length L with the alongchannel axis at an angle θ to the x axis. Further suppose that $W/L \ll 1$, so that ∂_{ll} derivatives can be neglected in comparison with ∂_{nn} derivatives in the barotropic vorticity equation (2.4). Then, for Stommel friction of the form $\mathbf{F} = A_S \nabla_h \times (\psi \mathbf{k})$,

$$\frac{1}{(f_N - f_S)} \int_{RQP} \mathbf{F} \cdot d\mathbf{l} \approx -r \delta_S \psi_n |_{n=W}$$

$$\approx -\frac{r}{2}\left(\coth \frac{\delta}{2} - 1\right),$$

where $\delta_S \equiv A_S/(\beta \sin\theta)$, $\delta \equiv W/\delta_S$, and $r \equiv (y_{N''} - y_{S''})/(y_N - y_S)$ is the ratio of the latitudinal extent of RQP to that of the island (see Fig. 5). Hence, substituting in (4.1) gives

$$\psi_0 \approx \left\{1 + \frac{r}{(e^\delta - 1)}\right\}^{-1} \psi_{max}. \qquad (4.2)$$

If the channel width is much narrower than the Stommel boundary-layer width, that is, $\delta \ll 1$, then (4.2) reduces to

$$\psi_0(t) \approx \frac{\psi_{max}}{(1 + r/\delta)}. \qquad (4.3)$$

A similar calculation can be performed for Munk friction, where $\mathbf{F} = -A_M \nabla_h^2(\nabla_h \times (\psi \mathbf{k})$. If $W/L \ll 1$, and no-slip boundary conditions ($\psi_n = 0$ on $n = 0$, W) are adopted, then

$$\frac{1}{(f_N - f_S)} \int_{RQP} \mathbf{F} \cdot d\mathbf{l} \approx r \delta_M^3 \psi_{nnn} |_{n=W},$$

$$\approx \frac{r}{2}\left\{\frac{e^{\delta/2}(c + s\sqrt{3}) - e^{-\delta}}{c\mathcal{C} + \sqrt{3}s\mathcal{S} - \cosh\delta}\right\}\psi_0,$$

where $\delta_M \equiv (A_M/\beta \sin\theta)^{1/3}$, $c = \cos(\sqrt{3}\delta/2)$, $s = \sin(\sqrt{3}\delta/2)$, $\mathcal{C} = \cosh(\delta/2)$, $\mathcal{S} = \sinh(\delta/2)$, and now $\delta \equiv W/\delta_M$. Hence, substituting in (4.1) gives

$$\psi_0 \approx \left\{1 + \frac{r}{2}\left[\frac{e^{\delta/2}(c + s\sqrt{3}) - e^{-\delta}}{\cosh\delta - c\mathcal{C} - s\sqrt{3}\mathcal{S}}\right]\right\}^{-1} \psi_{max}. \qquad (4.4)$$

If the channel width is much less than the Munk boundary-layer width, that is, $\delta \ll 1$, then (4.4) reduces to

$$\psi_0(t) \approx \frac{\psi_{max}}{(1 + 12r\delta^{-3})}. \qquad (4.5)$$

If free-slip boundary conditions ($\psi_{nn} = 0$ on $n = 0$, W) are adopted, then

$$\frac{1}{(f_N - f_S)} \int_{RQP} \mathbf{F} \cdot d\mathbf{l} \approx r \delta_M^3(\psi_{nnn} - \psi_{lln})|_{n=W}.$$

For long, narrow channels, that is, $W/L \ll 1$, $\delta \leqslant O(1)$, the contribution from ψ_{lln} will dominate that from ψ_{nnn}, so the problem must be solved in full. In general, the frictional reduction is negligible compared with that for no-slip conditions for the same parameter values.

c. Application to the Indonesian throughflow

Figure 6, which shows the geometry of the Indonesian seas used in the $1/2° \times 1/2°$ GCM described later in section 5, illustrates the difficulty in estimating L, W for the region. The relevant channels are all those in which the western boundary current rubs up against the west coast (or, e.g., 200-m isobath) of the many islands. As the importance of the friction calculation is to establish whether frictional effects are likely to be sufficiently large to reduce the throughflow to a negligible size, it is useful to consider a range of parameters. An upper limit on r is given by assuming the frictional channel extends from the equator to 12°S. Hence, assuming Australia–PNG extends 45° of latitude, then an upper limit on r is 0.3. The oceans' western boundary currents are observed to be of the order of 50 km wide, corresponding to a friction coefficient A_S of 1/ (10 days) for $\beta \sim 2 \times 10^{-11}$ m^{-1} s^{-1}. Except for Lombok Strait and a section of the Makassar Strait, which are of order 70 km wide, most of the passages are in excess of 100 km wide. Therefore, taking $\delta \sim 1$, $r \sim 0.3$ and substituting in (4.2) yields a frictional reduction of 15% on ψ_{max}. If δ were only 1/2, because of a larger friction coefficient or a smaller channel width, then the reduction would be 30% for $r \sim 0.3$. The reduction would be as high as 75% only if $\delta \sim 0.1$. A western boundary-layer width of 50 km corresponds to a Munk friction coefficient of $A_M = 5 \times 10^3$ m^2 s^{-1}. Taking $\delta \sim 1$, $r \sim 0.3$ and substituting in (4.4), gives a reduction in throughflow of 77%. This contrasts with a Stommel parameterization for the same parameter values. From (4.3), the reduction goes as δ^{-1} for Stommel friction, but from (4.5), the reduction goes as δ^{-3} for Munk friction as δ tends to zero. If $\delta \sim 2$, then the reduction due to Munk friction would be 23%. The no-slip boundary condition produces a very strong frictional effect, and therefore a large reduction in throughflow, for channels as narrow as the Munk width. Observational evidence, discussed in the next subsection, indicates that the throughflow is unlikely to be reduced by $O(75\%)$ over the Sverdrup estimate of 16 Sv. This implies that numerical models, for example, GCMs, of the region using Munk friction and no-slip boundary conditions could considerably underestimate the throughflow unless care is taken in
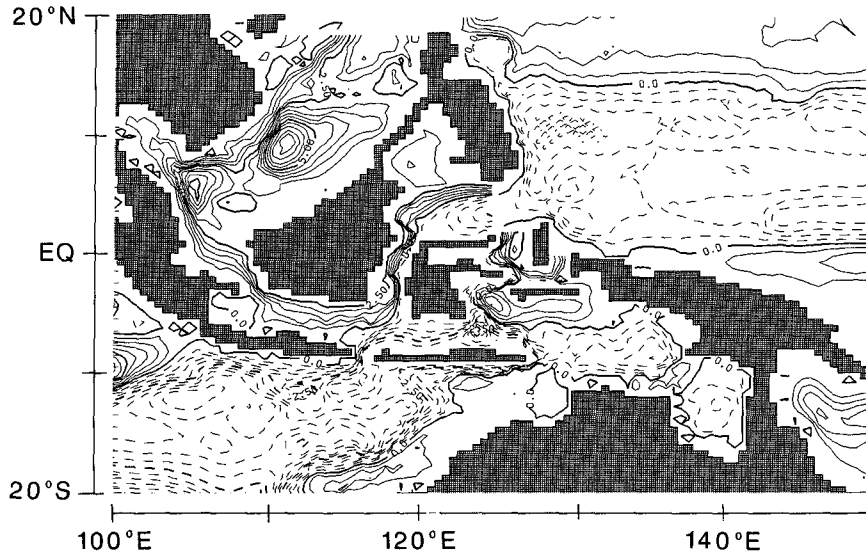
FIG. 6. The barotropic streamfunction during July in a GCM of the tropical Indian and Pacific oceans designed for ENSO simulations. The contour interval is 5 Sv in the Pacific Ocean and 0.5 Sv elsewhere. The instantaneous value of ψ on each island is Borneo/Philippines: 2.8 Sv, Lombok/Flores/Timor: -3.5 Sv, Sulawesi: -0.8 Sv, Sulu: 0.9 Sv, Halmahera: 2.2 Sv. The value on Asia and Australia–PNG is set to 0 for all time.

specifying a geometry/topography suitable for the spatial resolution.

d. Depth-integrated pressure differences

For the equilibrium response to a steady wind stress, the friction term in (4.1) may be estimated from measurements of the depth-averaged pressure difference. Integrating (2.8) along RQP (see Fig. 5a) gives

$$\int_{\text{RQP}} \mathbf{F} \cdot \mathbf{d}l = H_0 \Delta P_{\text{EAST}} - \int_{\text{RQP}} \frac{\boldsymbol{\tau}}{\rho_o} \cdot \mathbf{d}l \equiv H_0 \Delta P_{\text{EXCESS}},$$

and so substituting in (4.1) gives

$$\psi_0 = \frac{-1}{(f_N - f_S)} \oint_{\partial D + \partial I} \frac{\boldsymbol{\tau} \cdot \mathbf{d}l}{\rho_o} + \frac{H_0 \Delta P_{\text{EXCESS}}}{(f_N - f_S)}. \quad (4.6)$$

In this case, the pressure difference between the Pacific and Indian oceans along the eastern boundary is a measure of the throughflow magnitude in the sense that it measures the reduction from the maximum achievable for a wide channel, ignoring topographic effects. From Godfrey's (1989) Fig. 6a, the depth-integrated steric height decrease, relative to 1500 mb, from the Pacific entrance of the Indonesian archipelago to Sumatra, $H\Delta P/g$ is 50 m^2 at most. Godfrey also states that there is an increase from Sumatra to west Australia of 30 m^2, implying a drop along the west Australia coast of 20 m^2. In the annual mean, the alongshore wind stress is very weak. Therefore, from (4.6), the reduction in throughflow is $H\Delta P/(f_N - f_S)$ $\sim$ 2 Sv or 12% for $f_N \approx 0$, $f_S \approx f(45°\text{S})$. If $\mathcal{P}\nabla_h H$ enhancement is ignored, then this reduction can be

taken as a measure of frictional effects. If $\mathcal{P}\nabla_h H$ effects give a depth-integrated steric height increase of 50 m^2 equivalent to an increase in throughflow of 5 Sv, then the reduction due to frictional effects would be as high as 70 m^2 or 7 Sv, that is, 40%.

The expression (3.7) is unchanged in this case, and (3.8') becomes

$$H_0(\Delta P_{\text{WEST}} - \Delta P_{\text{EAST}})$$
$$= -(f_N - f_{S'})\psi_o + \int_{\text{FG+BE}} \frac{\boldsymbol{\tau}(x, y)}{\rho_o} \cdot \mathbf{d}l.$$

The unsuitability of this type of expression for investigating the throughflow is even more apparent if frictional effects are important, since then the pressure differences between the west and east sides of the archipelago entrances and exits will be even smaller.

e. Topographic effects

Expressions similar to (4.2) and (4.4) can be obtained for variable bottom topography with ψ_{max} given by (3.9). In deriving (4.2), (4.4), it was assumed that the frictional effects due to the alongchannel gradient in ψ were negligible in comparison with those based on the cross-channel gradient. However, if the along-channel topography varies on a scale giving similar gradients in ψ, a further correction would be needed.

f. Diagnosing interannual variations in the Indonesian throughflow

A final consideration is that the throughflow transport may be great enough that on passing over a nar-

row, shallow sill the flow will be accelerated sufficiently to make the nonlinear momentum terms neglected in (2.2) important. Also the flow could achieve critical speeds, and internal hydraulic jumps occur. The complex dynamics of the Indonesian seas suggests describing the throughflow in terms of the depth-averaged pressure difference between the Pacific and Indian oceans, but carrying out an integral around the Pacific as in establishing the island rule. Assuming topographic and nonlinear effects are negligible outside the Indonesian seas, then (4.6) is obtained, where now ΔP_{EXCESS} is interpreted as the depth-averaged pressure difference on the Australian continent between the northern entrance and southern exit in excess of that required to balance the alongshore wind stress. Nothing has been said about dynamics within the Indonesian seas; the pressure difference could be due to frictional dissipation, hydraulic, or $\mathcal{P}\nabla_h H$ effects.

Equation (4.6) is expressed as the equilibrium solution for a steady wind forcing and buoyancy forcing. However, the only approximations made in neglecting the time derivatives in its derivation were that the wind forcing and $\mathcal{P}\nabla_h H$ forcing in (2.4) occur in the global domain on time scales greater than the barotropic-to-pographic Rossby adjustment scale, and that P on the Australian–PNG coast had equilibrated, and that the western boundary layer had equilibrated. The decay time scale for equatorial waves is of order 2 years, but that for coastal trapped Kelvin waves is of the order of months. Also, their phase speed decreases with increasing latitude. Therefore, the adjustment time scale for P on Australia–PNG, which intersects the equatorial waveguide, is that for coastal Kelvin waves to propagate around Australia–PNG and across the Pacific and back. For a first baroclinic mode wavespeed of 3 m s^{-1}, an Australia–PNG boundary of 170° of latitude and Pacific Ocean width of 140° of latitude, this is about 280 days. Therefore (4.6) is a possible diagnostic relationship for investigating the depth-averaged throughflow on interannual time scales and longer. It has advantages over the equivalent "local" formulas (3.7) and (3.8′), as it separates the throughflow variability into two fundamental components. The first is the wind stress integral around the South Pacific, which drives the throughflow. Although, the Sverdrup gyres close in a complex fashion by the Philippine coast so that the throughflow appears to be of North Pacific origin, the dynamical source is the South Pacific wind stress curl; there could be a throughflow in the absence of the Mindanao Current, but not the South Equatorial Current. The second component is the pressure drop from the tip of Iria-Jaya along the west Australian coast in excess of that required to balance the alongshore wind stress, and so is a "local" forcing. The $\mathcal{P}\nabla_h H$ effect will typically give a depth-integrated pressure increase across the archipelago, whereas frictional and hydraulic effects will give a decrease.

Godfrey (1989) calculated the depth-integrated steric heights, relative to various depths, along the oceans' eastern boundaries from Levitus' (1982) climatological hydrology. He compared them with those obtained from his Sverdrup model driven by Hellerman and Rosenstein's (1983) climatological wind stress (see his Fig. 8). He found good agreement, and specifically it was much better than if he assumed the throughflow was blocked off in his Sverdrup model. There was a tendency for all the boundaries to show a greater variation in depth-integrated steric height than that required to balance the alongshore wind stress. This suggests that one may want to take into account frictional effects along eastern boundaries other than those due to the proximity of the western boundary. In which case, ΔP_{EXCESS} in (4.6) would be interpreted as $\Delta P_{EAST}(Australia) - \Delta P_{EAST}(South\ America)$, where ΔP is measured from the latitude of the northern tip of PNG to the latitude of the southern tip of Australia. The error bars on Godfrey's Fig. 8 are sufficiently large that one could choose a value of the total excess depth-integrated pressure drop along the west coast of South America and Australia–PNG, within the error limits, that would be sufficient to cancel a large portion of the throughflow. If frictional effects were so large, then nonlinearity in the equatorial currents or East Australia Current, not taken into account in the present theory, must overcome the reduction, as observational evidence does point to a throughflow of order 10 Sv.

5. Dynamical aspects of the Indonesian seas

Ultimately, the calculation of variations in the throughflow due to the variation in the Pacific wind stress, that is, (3.3), is a straightforward exercise given quality wind-stress data. A more challenging task is to understand the dynamics within the Indonesian seas and how they will affect the throughflow as described by (4.6).

An indication of the complexities of the flow in the Indonesian seas can be appreciated from some results already available from ENSO studies. Figure 6 shows the barotropic streamfunction in July from a Bryan-Cox numerical general circulation model (Cox 1984) used in the TOGA-NEG intercomparison by Prof. T. Yamagata and Y. Masumoto (personal communication). The GCM was forced by Hellerman and Rosenstein (1983) monthly mean wind stresses and a climatological surface heat flux based on Oberhuber (1988), which has a locally defined feedback if the sea surface temperature exceeds the climatology. The GCM was not designed to model the throughflow having temperature as the only thermodynamic variable, and indeed it was a limited domain; therefore, ψ on Australia–PNG was set to the Asian continent value of 0. Circulation was permitted around the various islands. The basic zonal pressure gradient balancing the equatorial zonal wind stress develops across both the Pacific and Indian Oceans, so the velocity field in the upper

levels is realistic, though details may differ within the Indonesian seas. The model has $1/2°$ × $1/2°$ resolution with 20 levels in the vertical. There were 10 levels in the upper 200 m; the other 10 were distributed down to 4000 m. The bottom topography, as specified at grid points for the prognosis of temperature (and salinity), was derived from an $1/8°$ × $1/8°$ dataset. In the rugged domain of the Indonesian seas, averaging of the topography in the prognosis of the horizontal velocity field makes parts of the various straits shallower and narrower at depth than they may be in practice, but this is not necessarily unrealistic dynamically. The model simulates the seasonal cycle in the upper Pacific Ocean very well, but less so that of the Indian Ocean. For the present purpose of illustration of various processes, this is not of concern.

Figure 6 shows the complex fashion in which the wind-driven gyres of the west Pacific close. The circulation around each island is small (<4 Sv) throughout the year, consistent with the multiple island rule (3.6) and their being sheltered from the Pacific Sverdrup flow. The relatively large circulation around Halmahera and Borneo–Philippines is because of their exposure to the Pacific wind-driven flow. The circulation around Lombok has a similar magnitude, but this is due to the differing sill depths connecting the island to Java and Australia and the large density gradient, which develops between the island's northern and southern boundaries. There is considerable recirculation of the Mindanao Current in the Celebes Sea, well in excess of that required to feed the flow through the Makassar Strait. Such a feature would be expected to carry through to a full model, and is likely to contribute to the freshness of the throughflow, as noted by Wajsowicz (1993a). The net transport through much of the seas is as a western boundary current, but the Makassar and Lombok straits, the straits around Halmahera, and that between Java and Borneo are notable exceptions. Also, in the Java and Flores Sea, the zonal flow is quite uniformly distributed, and not a narrow zonal jet as Sverdrup theory with simple western boundary-layer dynamics would predict. The lateral viscosity coefficient $A_M = 2 \times 10^3$ m^2 s^{-1}, so the Munk boundary width $(A_M/\beta)^{1/3} \approx 46.5$ km. Hence, the frictional reduction to the throughflow should be about 20% as given by (4.4) with $\delta \sim 2$, $r \sim 0.3$. Looking at Fig. 6, the quite uniform variation in ψ across the narrower straits suggests that δ may be effectively as low as 1, due to the resolution at depth of the V-shaped channels. In which case, the model could have a throughflow reduction as large as 75%, taking $r \sim 0.3$. Until it is computationally feasible to carry out interannual investigations using a much finer-resolution GCM, it would seem better to adopt free-slip boundary conditions to reduce the effect of friction.

Much of the throughflow is supposed to pass through the Makassar Strait. Figure 7 shows a vertical section of the meridional velocity and isotherms through the Makassar Strait in July. Unlike the section reproduced

in Hughes (1981) of a section from the 1938 *Snellius* expedition, the isotherms (or, in this model, isopycnals) go through considerable vertical excursions. It may be attributable to variations in local surface heat flux, but it suggests considerable modification due to vertical mixing and/or a pressure response to an accelerating flow. The isotherms are particularly jagged at the narrowest and shallowest part of the Makassar Strait ($2.5°$–$3°$S in Figs. 7a,b) and at the northern entrance to the Makassar Strait ($1°$–$1.5°$N in Fig. 7c), as part of the flow crosses a very shallow sill. A similar feature can be found through the late fall. In winter the flow is as fast, but the vertical shear is not so large, and the isotherms just dip on crossing the sill. It is reminiscent of two-layer hydraulics. If the flow accelerates to a critical speed on the sill, then the flow is unstable to long-wave perturbations if the difference in flow speed between the two layers is greater than $(gH)^{1/2}$, otherwise it will be hydraulically controlled, see Wajsowicz (1993b) for illustrations. In the model, the flow is accelerated to speeds in excess of 0.5 m s^{-1} over shelves as shallow as 100 m, which suggests that the flow could become critical over deeper sills in a full model or if shorter time scale fluctuations were included. Wyrtki (1961) observed surface currents of order 0.5–0.75 m s^{-1} in the Makassar Strait. The modeled flow through Lombok Strait exceeded 0.5 m s^{-1} except through the Northern Hemisphere winter. Similar speeds were observed by Murray and Arief (1988).

To estimate the channel width for which the throughflow would become critical, suppose there is a transport of $\psi \sim 15$ Sv over a sill of total depth $h \sim 200$ m and a lower-layer depth $h_2 \sim 100$ m. The flow will reach critical speeds (the composite Froude number ≥ 1) for strait widths

$$W \leqslant \frac{\psi}{g'h}\left(\frac{1}{h_1^2} + \frac{1}{h_2^2}\right)^{1/2},$$

which is ~ 25 km for a reduced gravity, $g' \sim 0.004\ g$. In the absence of dissipation, if the flow is nonlinear and subcritical throughout its passage along the strait, then the isotherms should dip, corresponding to a decrease in pressure, and then return to their former level on passing over a sill. If the flow becomes critical on a sill, then the isotherms will not return to their upstream level. A hydraulic jump will occur through which the flow is matched to its downstream values. In the presence of dissipation, the behavior will depend on the exact parameterization as described in Wajsowicz (1993b). For dissipation in the form of Laplacian viscosity in the momentum equations, the isotherms will recover their upstream depth, but this will be increasingly further downstream as the viscosity coefficient is increased. For bottom friction in the form of a quadratic drag, there is an irreversible pressure drop across a sill even for subcritical flows. In terms of the throughflow, it is just this steady-state pressure drop, which can be supported by friction, that will determine the modification to the throughflow.
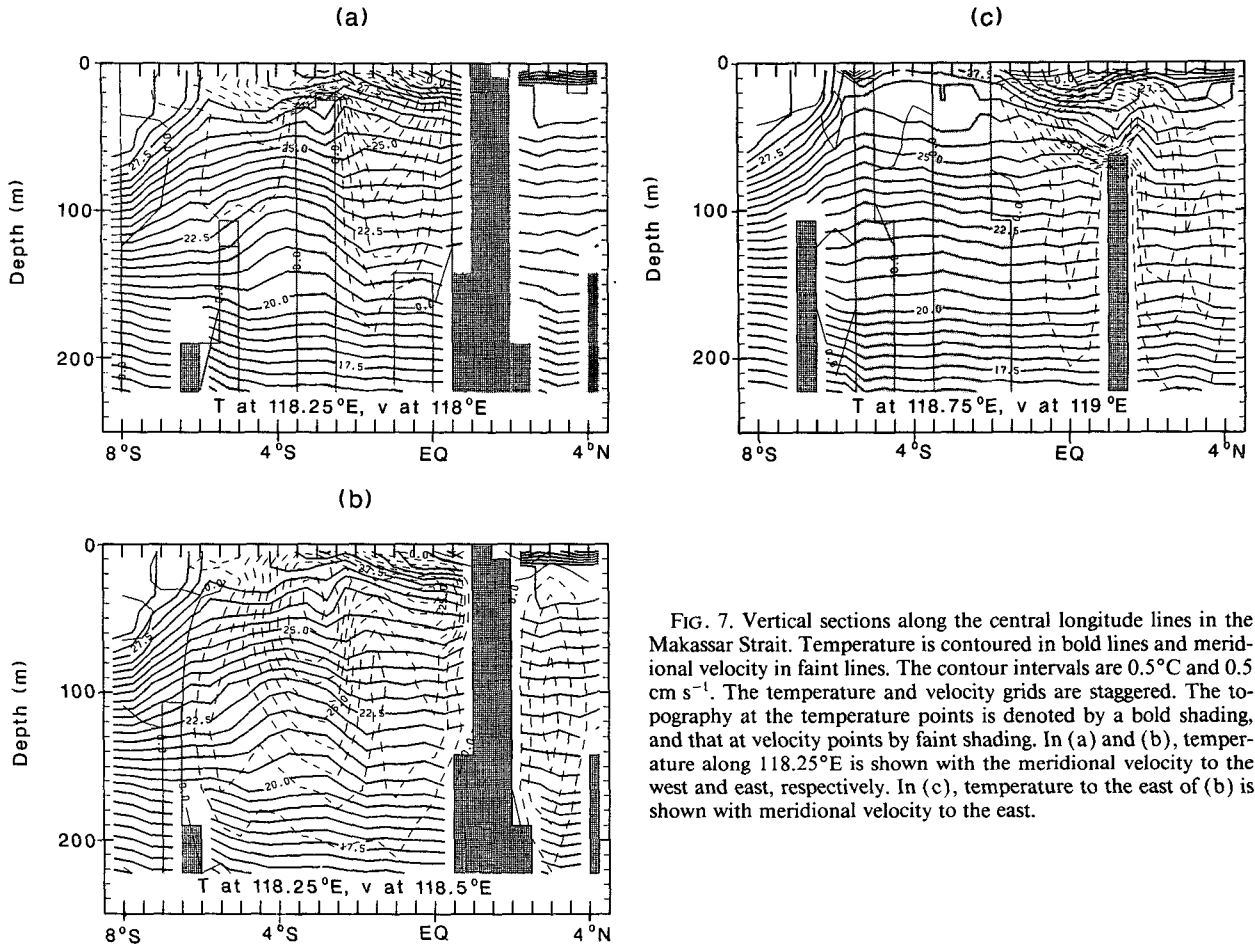
(a)

(b)

(c)

FIG. 7. Vertical sections along the central longitude lines in the Makassar Strait. Temperature is contoured in bold lines and meridional velocity in faint lines. The contour intervals are 0.5°C and 0.5 cm s^{-1}. The temperature and velocity grids are staggered. The topography at the temperature points is denoted by a bold shading, and that at velocity points by faint shading. In (a) and (b), temperature along 118.25°E is shown with the meridional velocity to the west and east, respectively. In (c), temperature to the east of (b) is shown with meridional velocity to the east.

The final figure shows the zonally averaged meridional streamfunction, Ψ between the tip of Iria-Jaya and the Lombok Strait for July (see Fig. 8a). In summer, the circulation is confined to above the effective depth of the Timor passage, and most is confined to above 200 m. In winter, the circulation pattern is reversed, and there is also a gyre below 500 m of $\sim$2 Sv, which upwells at the sills of the southern exit and returns northward. The pattern for heat transport is very similar. A first sight, the circulation in Fig. 8 is quite surprising. In summer, when the water is cooler in the south than the north, one expects there to be southward flow of the warm surface waters with a northward flow of the cooler waters at depth. The lack of this circulation in Fig. 8a emphasizes the importance of the depth-averaged circulation and zonal variation in topographic gradient across the Indonesian seas. In terms of the streamfunction ψ and baroclinic meridional velocity $\hat{v}$, the meridional overturning streamfunction is

$$\Psi(y, z) = \int_z^0 \int_{X_1(y)}^{X_2(y)} \hat{v} \, dx dz + \int_z^0 \int_{X_1(y)}^{X_2(y)} \frac{\psi_x}{H} \, dx dz.$$

(5.1)

Supposing $\hat{v}_z \approx -g\rho_x/f$ (or its nonrotating equivalent)

gives the classical picture of a thermohaline circulation previously described. A simple example illustrates the second term. Suppose $\psi = \psi_0$ on an island between two boundaries on which $\psi = \psi_1$ and $\psi = \psi_2$, respectively. Suppose the topography is flat between the island and each boundary, but the connecting sills are of differing depths H_1, $H_2(>H_1)$, respectively, then

$$\int_z^0 \int_{X_1(y)}^{X_2(y)} \frac{\psi_x}{H} \, dxdz$$

$$= \begin{cases} \left[\frac{\psi_1}{H_1} + \left(\frac{1}{H_2} - \frac{1}{H_1} \right)\psi_0 - \frac{\psi_2}{H_2} \right]z & -H_1 < z < 0 \\[2ex] \frac{H_1}{H_2}\psi_2 + \left(1 - \frac{H_1}{H_2} \right)\psi_0 - \psi_1 & \\[2ex] \quad - \frac{(\psi_2 - \psi_0)}{H_2}(z + H_1), & -H_2 < z \leqslant -H_1, \end{cases}$$

which varies linearly with z and has a discontinuity in gradient at $z = -H_1$. A decomposition of Ψ in terms of the contribution from the baroclinic and barotropic velocity fields is shown in Figs. 8b, c. The sections where the fields are similar but of opposite sign show the
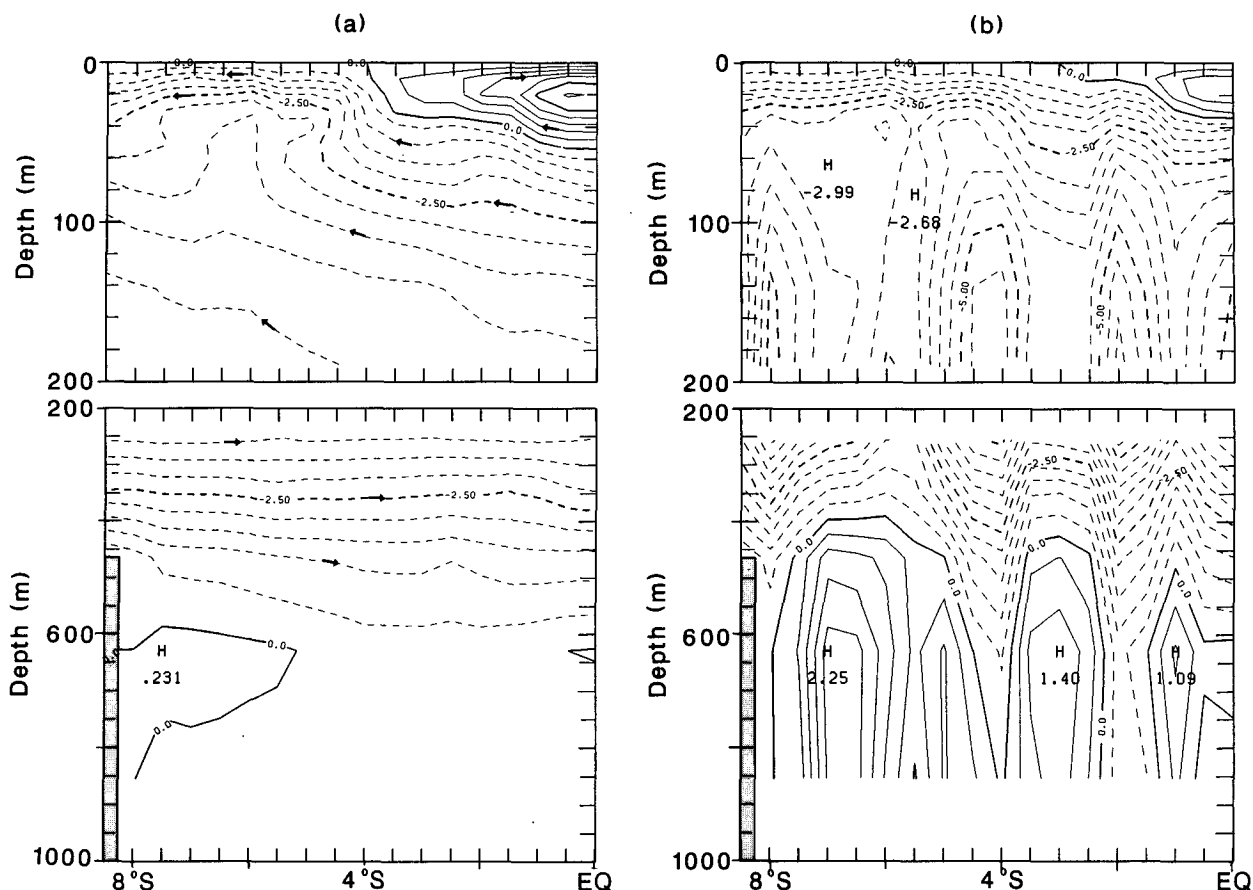
FIG. 8. The instantaneous zonally averaged meridional streamfunction during July for the section between the Asian continent and Australia–PNG is contoured in (a), with interval 0.5 Sv. The components for the baroclinic and barotropic flow as given by (5.1) are contoured in (b) and (c), respectively, with the same interval. The topography extends to depths in excess of 2000 m in places along 8°–9°S on the T–S grid. On the u–v grid there is an effective maximum sill depth of 460 m, denoted by the light shading.

baroclinic field adjusting to cancel the barotropic flow below the depths of the sills, or vice versa, see Wajsowicz (1991). Referring to the local geometry and topography, the various extrema in Fig. 8c correspond to the various islands and differing sill depths on either side. The surface-trapped feature of the circulation is attributable to the relatively large circulation around Borneo and the relative shallowness of the Java seas. This could be of even more significance in a full model, and suggests it would be wise to isolate Borneo from the Philippines, so that its circulation was not unduly influenced by the Sverdrup flow from the Pacific. From Fig. 8a, the zonally integrated southward flow into the Indian Ocean is only 4.5 Sv, which confirms the earlier calculation that the straits are frictional.

Figures 6 and 7 and the ensuing discussion described processes that could produce an irreversible pressure drop across the Indonesian archipelago and so affect the throughflow magnitude on interannual time scales as expressed by (4.6). The seasonal variation in throughflow magnitude cannot be expressed analytically, but the same processes are likely to limit the

magnitude on seasonal time scales as well. Although the ENSO-GCM was not designed to model the throughflow, study of its output has highlighted several modeling features that require further consideration. It also indicated that the zonally integrated meridional heat transport through the archipelago is influenced not only by the sill depths, but also by the zonal topographic gradient from Sumatra to Papua New Guinea.

6. Summary

An explicit theoretical estimate (3.3) of the circulation of the depth-averaged flow around a midocean island has been derived. It is valid for time scales greater than the barotropic Rossby adjustment time scale in a flat-bottomed ocean, or for time scales greater than baroclinic Rossby adjustment time scale in a variable-bottomed ocean, assuming a level of no motion can be specified above all the topography. A similar expression was derived by Godfrey (1989). An estimate of the reduction to the circulation was derived (4.1) if
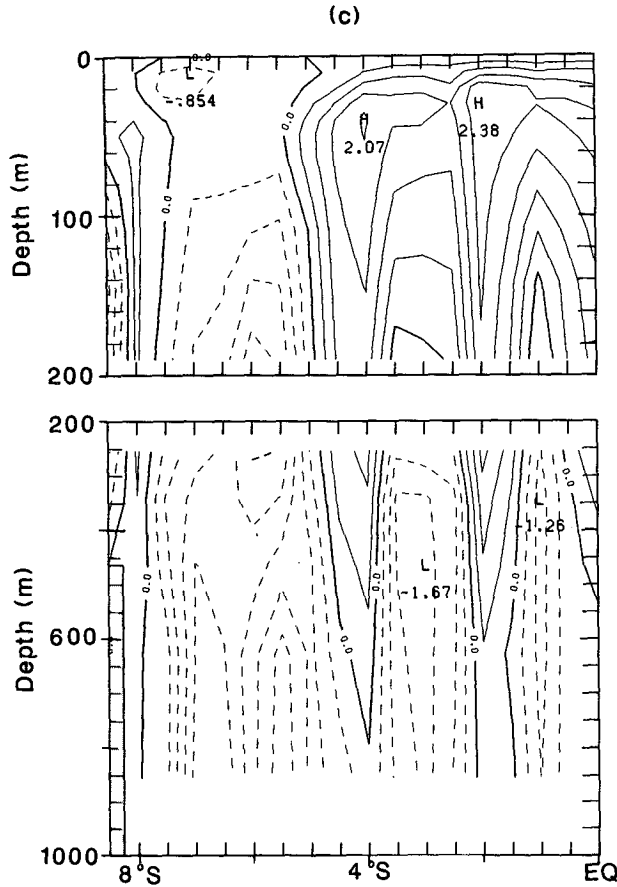
(c)

FIG. 8. (*Continued*)

the island lay within the basin's western boundary layer, so that frictional effects were important along its west coast as well. The modification to the island rule that allowed for explicit topographic variations was given in (3.9) and is valid for time scales greater than the barotropic–topographic Rossby adjustment time scale. A diagnostic expression (4.6) was proposed for investigating the interannual variations in the Indonesian throughflow. If there were a wide and deep channel between Australia and Asia, then the depth-integrated throughflow magnitude would be independent of conditions in the Indian Ocean. If the channel is narrow and shallow, such that frictional and nonlinear effects are important, then the Indian Ocean may exert an influence. Whether the variations are in the Pacific or Indian Ocean, the dynamics of the Indonesian seas and their ability to prevent coastal Kelvin waves from smoothing out the density gradient between the Pacific and Indian oceans along the Australian–PNG coast beyond that required to balance the alongshore wind stress will play an important role in determining the throughflow magnitude and variability. This latter aspect has received little attention and merits further study.

APPENDIX

Uniqueness of the Solution to the Barotropic Vorticity Equation in a Multiple-Connected Domain

For simplicity, only the case of a flat-bottomed domain will be considered. Consider a closed basin with boundary ∂B containing an island with boundary ∂I. Suppose ψ_1, ψ_2 are two solutions of (2.4), which satisfy the boundary conditions $\psi_1 = 0 = \psi_2$ on ∂B and $\psi_1 = C_1(t)$, $\psi_2 = C_2(t)$ on ∂I, and (2.6). Then the function $\psi = \psi_1 - \psi_2$ satisfies the equation

$$\nabla_h^2 \psi_t + \beta \psi_x = \text{curl } \mathbf{F} \qquad (A1)$$

and boundary conditions

$$\psi = 0 \quad \text{on} \quad \partial B, \quad \psi = C(t) \quad \text{on} \quad \partial I, \quad (A2)$$

plus further conditions if $\mathbf{F}$ is a function of derivatives of ψ higher than the first. Also, from (2.6)

$$\oint_{\partial I} \nabla_h \psi_t \cdot \mathbf{n} \, dl = \oint_{\partial I} \mathbf{F} \cdot d\mathbf{l}. \qquad (A3)$$

Multiplying (A1) by ψ and integrating over the basin yields

$$\iint_{B-I} \frac{1}{2} \{(\nabla_h \psi)^2\}_t \, dS + C(t) \oint_{\partial I} \nabla_h \psi_t \cdot \mathbf{n} \, dl$$

$$= -C(t) \oint_{\partial I} \mathbf{F} \cdot d\mathbf{l} + \iint_{B-I} \nabla_h \psi \times \mathbf{F} \cdot \mathbf{k} \, dS, \quad (A4)$$

where Stokes' theorem and the boundary conditions (A2) have been applied. Substituting from (A3) in (A4) gives

$$\iint_{B-I} \frac{1}{2} \{(\nabla_h \psi)^2\}_t \, dS = -\iint_{B-I} \nabla_h \times \psi \mathbf{F} \, dS. \quad (A5)$$

To prove uniqueness, the form of $\mathbf{F}$ and any further boundary conditions are chosen so that the right-hand side of (A5) is negative unless $\nabla_h \psi$, or $\nabla_h^2 \psi$ is identically zero. Hence, considering the integral with time of (A5), there is a contradiction as the left-hand side is positive unless $\nabla_h \psi$ is identically zero. Therefore, ψ is identically zero everywhere, hence $C(t)$ is identically zero, and the solution to (2.4), (2.6) with the specified boundary conditions is unique.

REFERENCES

Clarke, A. J., 1991: On the reflection and transmission of low frequency energy at the irregular western Pacific Ocean boundary. *J. Geophys. Res.*, **96**(Suppl.), 3289–3305.

Cox, M. D., 1975: A baroclinic numerical model of the world ocean: Preliminary results. *Proc. Symp. Numerical Models of Ocean Circulation,* Durham, New Hampshire, 107–120.

——, 1984: A primitive equation, 3-dimensional model of the ocean. GFDL Ocean Group Tech. Rep. No. 1, Geophysical Fluid Dynamics Laboratory/NOAA, Princeton University, Princeton, NJ 08542.

Gill, A. E., and K. Bryan, 1971: Effects of geometry on the circulation of a three-dimensional Southern-Hemisphere ocean model. *Deep-Sea Res.,* **18,** 685–721.

Godfrey, J. S., 1989: A Sverdrup model of the depth-integrated flow for the World Ocean allowing for island circulations. *Geophys. Astrophys. Fluid Dyn.,* **45,** 89–112.

Gordon, A. L., 1986: Interocean exchange of thermocline waters. *J. Geophys. Res.,* **91**C, 5037–5046.

Hellerman, S., and M. Rosenstein, 1983: Normal monthly wind stress over the World Ocean with error estimates. *J. Phys. Oceanogr.,* **13,** 1093–1104.

Hirst, A. C., and J. S. Godfrey, 1993: The role of the Indonesian throughflow in a global ocean GCM. *J. Phys. Oceanogr.,* **23,** 1057–1086.

Hughes, R. L., 1981: On cross-equatorial flow within a channel with application to the Makassar Strait. *Dyn. Atm. Oceans,* **6,** 103–120.

Huthnance, J. M., 1984: Slope current and "JEBAR." *J. Phys. Oceanogr.,* **14,** 795–810.

Inoue, M., and S. E. Welsh, 1993: Modeling seasonal variability in the wind-driven upper-layer circulation in the Indo–Pacific region. *J. Phys. Oceanogr.,* **23,** in press.

Ishizaki, H., 1993: A simulation of the Abyssal Circulation in the North Pacific Ocean. *J. Phys. Oceanogr.,* submitted.

Kindle, J. C., H. E. Hurlburt, and E. J. Metzger, 1989: On the seasonal and interannual variability of the Pacific to Indian Ocean throughflow. *Proc. West Pacific Int. Meeting and Workshop on TOGA COARE, Noumea, New Caledonia,* 355–365.

Levitus, S., 1982: *Climatological atlas of the World Ocean.* NOAA Prof. Paper 13, U.S. Department of Commerce/National Oceanic and Atmosphere Administration, Rockville, Md., 173 pp.

Murray, S. P., and D. Arief, 1988: Throughflow into the Indian Ocean through the Lombok Strait, January 1985–January 1986. *Nature,* **333,** 444–447.

Oberhuber, J. M., 1988: An atlas based on the "COADS" Data Set. Rep. No. 15, Max Planck Institut fur Meteorologie, Hamburg, 199 pp.

Rhines, P. B., and P. MacCready, 1989: Boundary control over the large-scale circulation. *Parameterization of Small-scale Processes, Proc. Hawaiian Winter Workshop, University of Hawaii at Manoa,* 75–97.

Semtner, A. J., and R. M. Chervin, 1988: A simulation of the global ocean circulation with resolved eddies. *J. Geophys. Res.,* **93**C, 15 502–15 522.

Veronis, G., 1973: Model of world ocean circulation. Part 1: Wind-driven two-layer. *J. Mar. Res.,* **31,** 228–188.

Wajsowicz, R. C., 1991: On stratified flow over a ridge intersecting coastlines. *J. Phys. Oceanogr.,* **21,** 1407–1437.

——, 1993a: A simple model of the Indonesian throughflow and its composition. *J. Phys. Oceanogr.,* **23,** in press.

——, 1993b: Dissipative effects on inertial flows over a sill. *Dyn. Atmos. Oceans,* **17,** 257–301.

——, 1993c: A relationship between interannual variations in the South Pacific wind stress curl, the Indonesian throughflow, and the west Pacific warm water pool. *J. Phys. Oceanogr.,* submitted.

Wyrtki, K., 1961: Physical Oceanography of the Southeast Asian Waters. Scientific results of marine investigations of the South China Sea and Gulf of Thailand 1959–1961, NAGA Rep. No. 2, University of California, Scripps Institution of Oceanography, La Jolla, California, 195 pp.

——, 1987: Indonesian throughflow and the associated pressure gradient. *J. Geophys. Res.,* **92**C, 12 941–12 946.